

Mechanisms for catalytic carbon nanofiber growth studied by *ab initio* density functional theory calculations

Frank Abild-Pedersen and Jens K. Nørskov

Center for Atomic-scale Materials Physics, Department of Physics, NanoDTU, Building 307, Technical University of Denmark, DK-2800 Kgs. Lyngby, Denmark

Jens R. Rostrup-Nielsen, Jens Sehested, and Stig Helveg
Haldor Topsøe A/S, Nymøllevej 55, DK-2800 Kgs. Lyngby, Denmark

(Received 8 July 2005; revised manuscript received 30 November 2005; published 20 March 2006)

Mechanisms and energetics of graphene growth catalyzed by nickel nanoclusters were studied using *ab initio* density functional theory calculations. It is demonstrated that nickel step-edge sites act as the preferential growth centers for graphene layers on the nickel surface. Carbon is transported from the deposition site at the free nickel surface to the perimeter of the growing graphene layer via surface or subsurface diffusion. Three different processes are identified to govern the growth of graphene layers, depending on the termination of the graphene perimeter at the nickel surface, and it is argued how these processes may lead to different nanofiber structures. The proposed growth model is found to be in good agreement with previous findings.

DOI: 10.1103/PhysRevB.73.115419

PACS number(s): 31.15.Ew, 81.07.De, 82.65.+r

I. INTRODUCTION

The catalyzed formation of carbon nanofibers and nanotubes over supported metal nanoparticles has received much attention because it may provide low-cost, large-scale syntheses of carbon nanofibers or nanotubes,¹⁻⁴ and it is important to inhibit this in order to prevent breakdown of industrial steam reforming catalysts for the production of hydrogen and synthesis gas.⁵ Despite numerous studies, the growth mechanisms are still subject to intense debate. Often, the metal-catalyzed growth is explained by the following mechanism:⁶⁻⁸ (i) Carbon-containing compounds adsorb dissociatively at the surface of metal nanoclusters; (ii) carbon dissolves in the bulk of the metal cluster; (iii) carbon diffuses through the bulk of the metal nanocluster to the rear end, where (iv) the carbon atoms are incorporated into the new graphene layers of the growing nanofiber [Fig. 1(a)]. In this model, the bulk diffusion of carbon is driven by a carbon concentration gradient established between the gas-metal and metal-graphene interfaces. However, the specific role of the nanocluster surface has also been considered to be of importance, and therefore, growth models based on surface-mediated carbon transport have also been proposed⁹⁻¹² [Fig. 1(b)]. The debate reflects the challenge associated with revealing in detail the dynamic processes occurring during growth. *In situ* transmission electron microscopy (TEM) provides unique means for monitoring the formation of nanofibers or nanotubes and, hence, allows kinetic and mechanistic insight to be obtained.^{6,13,14}

Recently, *in situ* high resolution TEM (HRTEM) was used to obtain atomic-scale insight into the formation of multi-walled graphitic nanofibers by methane decomposition over nickel nanoclusters.¹⁵ The results revealed that the nucleation and growth of graphene layers are associated with the dynamic formation and restructuring of monoatomic step-edges at the nickel surface. An interplay with preliminary density functional theory (DFT) calculations indicated that the obser-

vations are consistent with a growth model involving surface transport of carbon and nickel atoms. Here, we present more extensive DFT calculations to address the mechanisms by which carbon can assemble into graphene layers or nanofibers at Ni surfaces.

The article is organized as follows: Section II provides a brief description of the experimental findings for multi-walled carbon nanofiber growth. Section III describes the theoretical framework. Section IV is divided into three parts: (1) the adsorption energies of carbon adatoms at different Ni sites are presented, (2) the different diffusion paths that carbon can follow from the adsorption site at the free nickel surface to the perimeter of a growing graphene layer are compared, and (3) the mechanism for incorporation of carbon atoms into the growing graphene layer is discussed. Section V provides a discussion of the results in the light of previously proposed growth models.

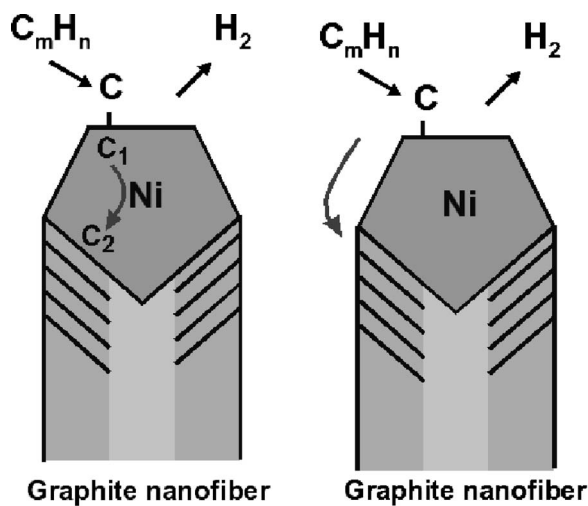


FIG. 1. Illustrations of growth mechanisms for multi-walled carbon nanofibers with carbon diffusion via (a) the Ni bulk (Ref. 8) and (b) the Ni surface.

II. ATOMIC-RESOLVED IMAGING OF MULTILAYERED CARBON NANOFIBER GROWTH

In a previous study, *in situ* HRTEM was used to monitor carbon nanofiber growth.¹⁵ The carbon nanofibers are formed by exposing oxide-supported nickel nanoclusters (with a diameter of 5 to 20 nm) to a 1:1 mixture of methane and hydrogen at about 2 mbar at a temperature of about 530 °C. The HRTEM images reveal that graphitic nanofibers grow with a Ni nanocluster at the front end and that the graphene layers are aligned into multi-walled carbon nanofiber structures with a morphology depending on a reaction-induced reshaping of the Ni nanocluster. It is observed that the smaller Ni particles tend to obtain an elongated shape and partial multi-walled carbon nanotubes form, and that the larger Ni particles tend to obtain a pear shape and whisker-type carbon nanofibers form with graphene layers inclined with respect to the fiber axis.

From the time-resolved *in situ* HRTEM image series, an interfacial growth mechanism was identified governing the formation of multilayered graphitic nanofibers. Figure 2 demonstrates the mechanism reported in Ref. 15: The HRTEM images reveal that monoatomic step-edges are induced spontaneously in the course of the reaction, even at the graphene-Ni interface. In between the pair of such step-edges, an additional graphene layer grows as the Ni step-edges move toward the ends of the Ni cluster and vanish. This process involves transport of C atoms toward and Ni atoms away from the graphene-Ni interface: The flux of Ni atoms is directed toward the free Ni surface to account for the continuous growth. Carbon atoms, resulting from methane decomposition at the free Ni surface, must diffuse to the interface to account for the growth of the graphene layer. Transport of nickel surface atoms must proceed via surface diffusion because the Ni particle remains crystalline during growth.

Consistent with this, preliminary DFT calculations show that nickel atoms are destabilized by more than 5 eV in bulk interstitial sites compared to adsorption in fcc sites on the Ni(111) surface, thus excluding any bulk interstitial self-diffusion. According to the DFT calculations, the main effect on the nickel transport from the graphene overlayer is a stabilizing contribution, which results in an increase in adsorption energy of nickel atoms at the interface. This effect will help the release of nickel atoms, promote further step-edge formation, and consequently ease the formation of new graphene layers at the nickel-graphene interface. The previous calculations consistently explain the observed spontaneous formation of nickel step-edges: Step-edge formation energies based on theoretical calculations report values of 0.41 eV and 0.16 eV per Ni step-edge atom,^{16,17} both less than the energy gained when binding carbon atoms to the step-edges.^{15,16} Since nickel transport may proceed along the graphene-nickel interface, it is likely that a similar transport mechanism can also account for the transport of carbon atoms. The previous DFT calculations indicated that this indeed is a possibility and the results presented in the following will substantiate this in greater detail.

III. CALCULATIONAL DETAILS

The self-consistent DFT total energy calculations were done using the generalized gradient approximation¹⁸ (GGA-

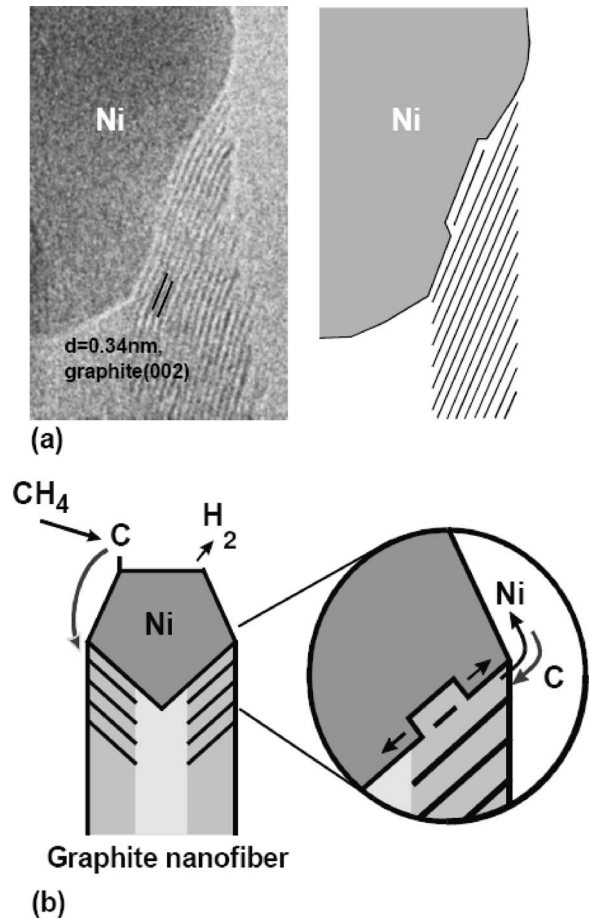


FIG. 2. (a) (left) *In situ* high-resolution transmission electron microscopy image, obtained during carbon nanofiber growth, showing the interface between the nickel nanoparticle and the carbon whisker (adapted from Ref. 15) and (right) schematic presentation of the graphene-nickel interface specifying the growth of a graphene layer between monoatomic Ni step sites at the nickel surface. (b) Illustration of the growth mechanism for carbon nanofibers established from the interplay of *in situ* HRTEM observations and DFT calculations.

RPBE). The Vanderbilt pseudopotential approximation was used to describe the ionic core electrons and their interaction with the valence electrons.¹⁹ The one-electron valence states were expanded in a plane wave basis with a kinetic cutoff energy of 25 Ry. The density of the valence electrons were determined self-consistently by an iterative diagonalization of the Kohn-Sham Hamiltonian²⁰ using Pulay mixing of densities. The Fermi occupation of the one-electron Kohn-Sham states was calculated at a temperature of $k_B T = 0.1$ eV. All total energy calculations were extrapolated to zero electronic temperature and performed with the magnetic moment of the nickel surface taken into account.

The surfaces of the Ni nanoclusters are represented by different Ni model surfaces. The plane surfaces are modeled by the close-packed Ni(111) surface of three-layer slabs with either $p(2 \times 2)$ or $p(3 \times 3)$ unit cells. Figure 3(a) shows the (111) slab with $p(2 \times 2)$ structure. The surface step-edges are modeled by the Ni(211) surface of a nine-layer slab or the Ni(322) surface of a fifteen-layer slab. The (211) and (322)

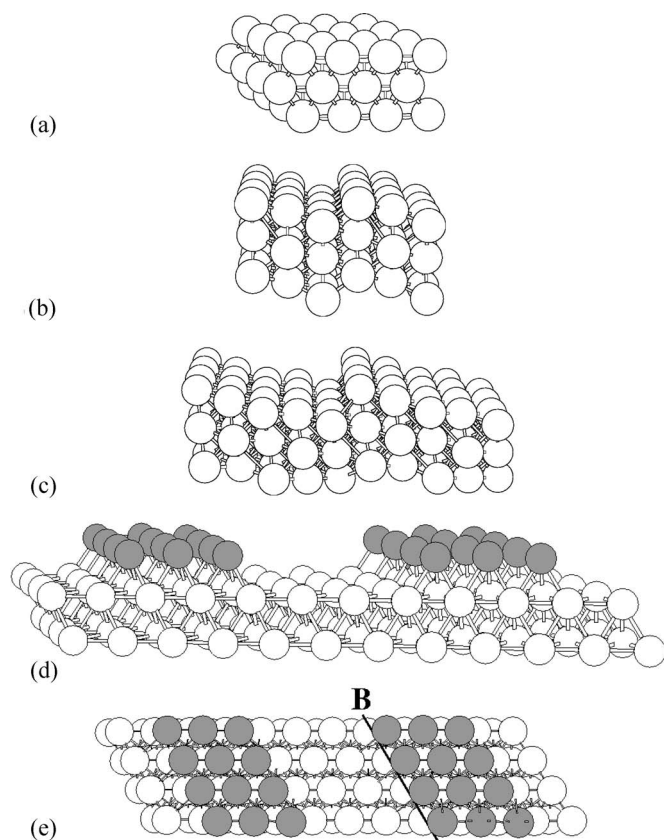


FIG. 3. The different nickel surface structures used in the DFT calculations. (a) A Ni(111) three-layer slab, (b) a Ni(211) nine-layer slab, (c) a Ni(322) fifteen-layer slab, and (d) a 6×2 Ni(111) three-layer slab with three atomic rows missing. (e) Top view of the 6×2 Ni(111) surface. The line along the step edge denoted by *B* contains the fivefold sites with a local (100) symmetry. The gray atoms are the surface Ni atoms forming the infinite islands. All unit cells are repeated twice in the two directions parallel to the surface.

models have step-edges with a local (100) geometry separated by (111) facets with a width of either three or five atomic rows [see Figs. 3(b) and 3(c)]. Both of the stepped model surfaces have a slab thickness comparable to the Ni(111) surfaces.

The graphene-nickel interface is modeled by a Ni(111) surface with a graphene overlayer. We find that the graphene overlayer is bound to the nickel surface through the weak van der Waals interaction. These interactions are poorly described in the generalized gradient approximations (GGAs) within DFT, whereas the local density approximation (LDA) gives a better description of these interactions.²¹ Using LDA, we obtain an adhesion energy of 0.05 eV per carbon atom and a metal-to-graphite binding distance of 3.22 Å, in fair agreement with experimental obtained distances of 2.8 Å.²² We stress that remaining total energy calculations have been done using the RPBE functional. This required a fixation of the graphene overlayer at the calculated distance of 3.22 Å in the direction perpendicular to the surface on clean Ni(111). In the cases where adatoms are located at the interface, metal atoms in the first surface layer, the adatoms in the middle layer, and the carbon atoms in the graphene overlayer are relaxed in all three spatial directions.

For computing the growth of graphene from a step edge, we have used a stepped Ni(322) surface, a 6×2 Ni(111) supercell with three atomic rows missing and a 8×2 Ni(111) supercell with five atomic rows missing. The last two form periodic structures with infinite islands three atomic rows wide separated by step-edges having the (100) symmetry. Figures 3(d) and 3(e) show the structure of the 6×2 supercell.

In the calculations, each of the slabs were separated by approximately 12 Å of vacuum. Nickel atoms in the first close-packed (111) layer of the surfaces were allowed to relax fully, whereas nickel atoms in the remaining layers were kept fixed in their bulk position with a calculated lattice constant of 3.518 Å. For the subsurface calculations, we used a $p(3 \times 3)$ unit cell of three layers. Nickel atoms in the two first surface layers were relaxed while the third layer was fixed.

We note that carbon binding energies found for the five-fold site on Ni(211), Ni(322), and the Ni(111) surfaces with missing rows only differ by 0.15 eV and that no significant difference between adsorption in threefold hollow hexagonal close-packed (hcp) sites of carbon on $p(2 \times 2)$ and $p(3 \times 3)$ Ni(111) is found. The bulk calculations were done using a $p(3 \times 3)$ unit cell of three layers, and all atoms were allowed to relax fully in the calculations. A sampling of $4 \times 4 \times 1$ special *k* points of the Monkhorst-Pack type²³ was used to model the first Brillouin zone for the (111) and (211) surfaces, a $3 \times 3 \times 3$ sampling was used for the bulk, and a $4 \times 2 \times 1$ sampling was used for the remaining surfaces.

We have located all barriers and transition states for the carbon diffusion steps and the incorporation of carbon atoms into perimeter sites of graphene using the nudged elastic band (NEB) method.²⁴ We have used 7–11 configurations along the reaction path, including endpoints, to describe the pathway between the different intermediate states. All configurations were relaxed until the change in energy was less than 0.002 eV.

IV. RESULTS

The following section is divided into three parts. In Sec. IV A, we present the calculated adsorption energies at different Ni sites. In Sec. IV B, we examine transport paths for carbon to migrate to perimeter sites of a graphene layer growing on the Ni surface or at the graphene-Ni interface. Specifically, we address transport mechanisms involving diffusion along the surface, in the subsurface layer, and through the bulk of the Ni nanocrystal. In Sec. IV C, we describe the growth of graphene layers. The graphene layer is suggested to nucleate at the step-edge sites and to grow out over the surrounding Ni facets as more carbon is added.¹⁶ The unsaturated sp^2 orbitals at the perimeter define two different types of sites at which carbon can be incorporated, i.e., perimeter sites located over the Ni(111) facet or at the Ni step edge. We identify three processes by which carbon adatoms are incorporated at the perimeter sites.

A. Energetics of carbon adsorption

Gaseous hydrocarbons adsorb dissociatively on Ni surfaces. The decomposition preferentially takes place in the

vicinity of low-coordinated metal surface atoms such as step-edge atoms.^{16,25,26} For methane, the activation of the first C-H bond is rate-limiting for the decomposition and it is associated with an activation energy barrier, obtained from DFT, of less than 1 eV at the undercoordinated step sites on Ni.^{16,27} The decomposition barrier is less than the barriers we identify for graphene growth, and methane decomposition will, therefore, not be considered further in the following.

The carbon atoms resulting from the decomposition can adsorb at various Ni sites. This section examines the carbon stability on the (111) facet without and with a graphene overlayer (models 1 and 4 in Table I), at the step-edges on Ni(211) for different carbon coverages (models 2 and 3), at the step edge with a graphene overlayer (model 6), in a graphene overlayer (model 5), and in subsurface (model 7) or bulk octahedral interstitial sites (model 8). The calculated adsorption energies are given in Table I.

The calculations show, in accordance with Ref. 16, that carbon obtains the lowest energy when incorporated in a graphene overlayer on the Ni(111) facet. Thus, there is an energetic driving force for incorporation of C atoms into the graphene layer from all of the considered nickel sites. To describe carbon adsorption on the surface of the Ni nanocrystals, we focus on the threefold hollow hcp sites on Ni(111) and the fivefold hollow sites on Ni(211). At the Ni(111) surface, the lowest energy adsorption site is the threefold hollow hcp site. The hcp site is only slightly favored over the fcc site by 0.05 eV. The calculations show that carbon binds more strongly at step-edge sites on Ni(211) than at hcp facet sites on Ni(111). This increase in adsorption energy of carbon at step-edge sites suggests that nucleation of graphene preferentially occurs at the step edge and that step-edge sites, therefore, play an important role for the growth of carbon nanofibers.¹⁶

We calculated the adsorption energies at two different coverages on Ni(211), $\theta_C = \frac{1}{6}$ (ML) and $\theta_C = \frac{1}{3}$ ML of carbon, corresponding to step-edge coverages of $\theta_C^{st} = \frac{1}{2}$ and $\theta_C^{st} = 1$. One monolayer (ML) is defined as the atomic density in the Ni(111) surface and θ_C^{st} is defined as the number of carbon atoms per Ni step-edge atom. The results presented in Table I show that there is a substantial repulsive interaction between the C atoms at the step-edges, but even at a coverage of $\theta_C^{st} = 1$ the step-edge site preference still persists.

We have also examined carbon adsorption at the nickel surface sites in the presence of a graphene overlayer, as a model for carbon adsorption at the graphene-nickel interface. We observe that a carbon atom at the hcp site on Ni(111) covered with a graphene layer is destabilized by 0.37 eV relative to the same site on a graphene-free Ni(111) surface. Carbon adsorbed in the fivefold hollow step-edge site terminated by a graphene layer, at a coverage of $\theta_C^{st} = \frac{1}{2}$, is destabilized by 0.65 eV as compared to carbon atoms at a graphene-free step-edge site with a similar coverage. Hence, the graphene overlayer has a destabilizing effect on the carbon adsorption at both step edge and facet sites. In the following sections, we consider $\theta_C^{st} = 1$ only, corresponding to a full saturation of carbon along the step edge.

For the octahedral interstitial bulk sites, we considered sites in the first subsurface layer of a Ni(111) surface and in

an infinite Ni bulk crystal. The calculations show that carbon adsorption in the first subsurface layer is more stable than in the bulk. For the bulk sites, the energy relative to the (111) surface is zero, indicating that there is no energetic driving force for incorporating carbon into the octahedral bulk nickel sites. Furthermore, the stability of the carbon atoms in the first subsurface layer is higher than at the facet sites but less at step-edge sites. This ranking of carbon stabilities suggests that the first subsurface layer could play a role in the surface dynamics. The increased stability of carbon in the subsurface site as compared to the facet site is due to the increase in coordination²⁹ to Ni and an outward elastic relaxation of the Ni surface layer. For C atoms adsorbed in the first subsurface layer, the Ni surface atoms relax outward by 0.2 Å as compared to their position in the fully relaxed clean Ni(111) surface. On the other hand, for carbon adsorbed in octahedral sites in bulk Ni, no elastic deformation of the Ni lattice is found in our calculations as compared to the fully relaxed, clean Ni bulk. This is attributed to the secondary Ni coordination shells, and the energy gain from relaxations is consequently smaller. A similar effect was observed previously in studies of subsurface oxygen in the late 4d transition metals.³⁰

B. Diffusion pathways of C adatoms

In this section, we consider different transport pathways that carbon atoms can follow along the Ni nanocluster. Specifically, we focus on diffusion paths from the preferred step-edge adsorption site at the graphene-free nickel surface to a facet site on the graphene-nickel interface. We calculate diffusion energy barriers for the elementary diffusion steps and combine these with the energetics from Sec. IV A, to establish the potential energy diagrams for C transport along the different paths. The energy barriers for the elementary displacement steps are given in Table II.

1. Transport of carbon on the nickel surface

In the simplest picture, transport of carbon can be viewed to follow a path from the Ni step site along the Ni surface, modeled by the free Ni(111) facet, to the graphene-nickel interface (see Fig. 4). This transport path consists of (i) the detachment of carbon atoms from a step site to a (111) facet site, (ii) carbon diffusion via the free Ni(111) surface to the perimeter at the graphene-nickel interface, (iii) incorporation at the interface, and (iv) diffusion along the interface. Figure 4 shows the corresponding potential energy diagram. The overall energy barrier for this transport path can be found as the sum of the energy contribution from steps (i), (iii), and (iv), and from this, we estimate the overall barrier to be 1.42 eV.³¹

Surface defects, like steps, must be present on the curved surface of the nickel nanoclusters during the experiment and may add to the diffusion energy barrier. The influence of defects on the surface transport mechanism is modeled by carbon diffusion across a graphene-free nickel step site. The migration over a nickel step site can proceed from the upper part of the step to the lower part at the free nickel surface or vice versa. However, due to a stronger binding of carbon at

TABLE I. Side (left) and top views (right) of the geometries modeled in the DFT calculations together with the carbon adsorption energies. In the models, the black spheres represent carbon and the white spheres represent nickel. We define the coverage θ_C^{st} as the ratio N/N_{tot} , where N is the number of carbon atoms adsorbed and N_{tot} is the total number of step-edge atoms. θ_C is given as the surface coverage in ML, where 1 ML is defined as the density in (111) surface atoms. θ_C^{slab} and θ_C^{bulk} are defined as the ratio between the total number of carbon atoms and the total number of Ni atoms in the unit cells. All energies are relative to atomic carbon adsorbed at the step edge on Ni(211) with $\theta_C^{st}=1$. Models 1–5 show four repetitions of the unit cell, model 6 shows two repetitions of the applied unit cell, model 8 shows a single unit cell, and model 7 displays parts of a unit cell. In models 7 and 8, several spheres are displayed as transparent to better pinpoint the exact octahedral adsorption sites in the subsurface and in the bulk of Ni. Furthermore, in model 8, the unit cell containing 27 bulk Ni atoms and the adsorbed carbon are illustrated by a dashed box. Figures have been displayed using visual molecular dynamics (Ref. 28).

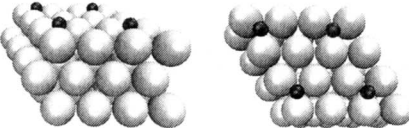
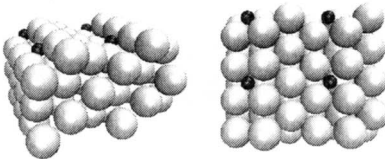
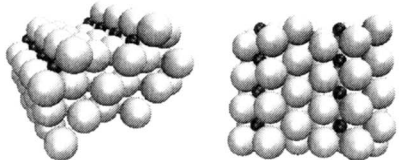
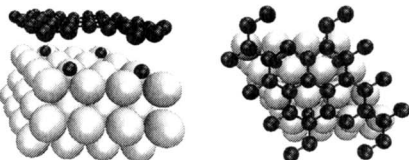
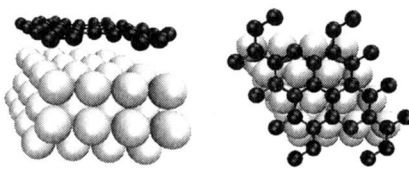
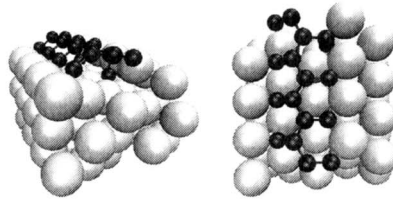
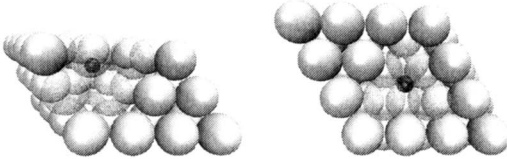
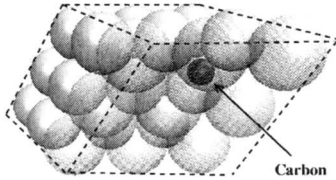
Structure	E_{ads} (eV)	Structure	E_{ads} (eV)
<p>1</p>  <p>Ni(111) hcp site with $\theta_C = \frac{1}{4}$ ML.</p>	0.55	<p>2</p>  <p>Ni(211) step-edge with $\theta_C^{st} = \frac{1}{2}$.</p>	-0.45
<p>3</p>  <p>Ni(211) step-edge site with $\theta_C^{st} = 1$.</p>	0.00	<p>4</p>  <p>Interface hcp site on Ni(111) with $\theta_C = \frac{1}{4}$ ML.</p>	0.92
<p>5</p>  <p>Infinite graphene layer.</p>	-0.75	<p>6</p>  <p>Interface site at step-edge with $\theta_C^{st} = \frac{1}{2}$.</p>	0.20
<p>7</p>  <p>Subsurface (octahedral site) with $\theta_C^{slab} = \frac{1}{27}$.</p>	0.21	<p>8</p>  <p>Bulk (octahedral site) with $\theta_C^{bulk} = \frac{1}{27}$.</p>	0.53

TABLE II. The first column indicates diffusion steps between different sites considered in Table I (site index given in parenthesis). The second column shows the corresponding energy barriers (given per carbon atom) as calculated from DFT.

Diffusion Step	E_{diff} (eV)
Clean surface (1) → clean surface (1)	0.50
Interface (4) → interface (4)	0.50
Step edge (3) → clean surface (1)	0.55
Clean surface (1) → subsurface (7)	1.00
Hcp step edge (1) → step edge (3)	0.75
Step edge (3) → subsurface (7)	0.75
Subsurface (7) → subsurface (7)	0.80
Subsurface (7) → interface (4)	1.34
Bulk (8) → bulk (8)	1.80

the lower part of the step, diffusion from the upper terrace must be associated with the lowest barrier, and this path will, therefore, be considered. For a direct step down, the carbon atom will migrate from a threefold hollow site above the step through a bridge site at the step edge and finally adsorb into

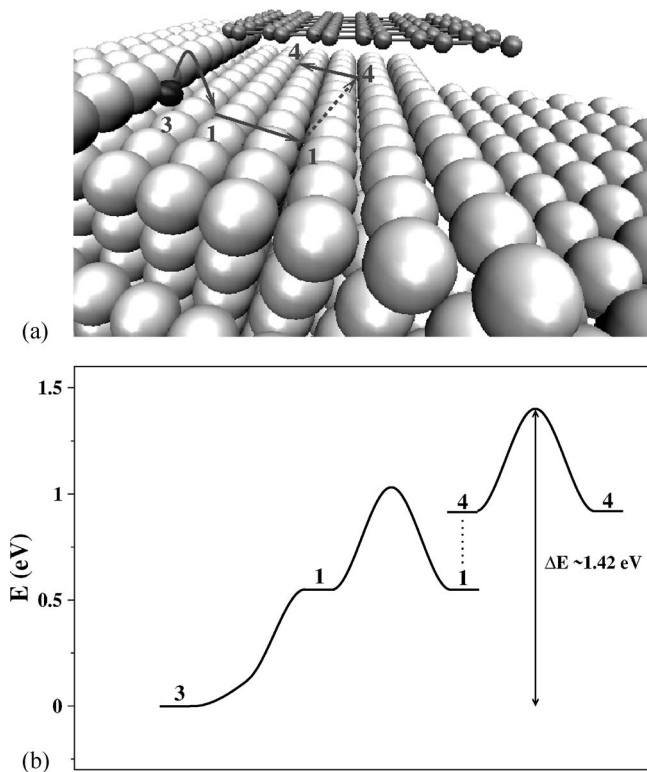


FIG. 4. (a) An illustration of the C diffusion steps on the Ni surface including facet and interface diffusion. The light gray spheres constitute the graphite overlayer, whereas the dark gray sphere indicates the surface carbon adatom in its most favorable surface site. The white spheres indicate surface nickel atoms. The site numbering corresponds to the models in Table I. The dotted line indicates the diffusion of carbon from the clean facet to the interface. (b) The calculated potential energy diagram for the C transport path in (a) with an indication of the overall transport energy barrier.

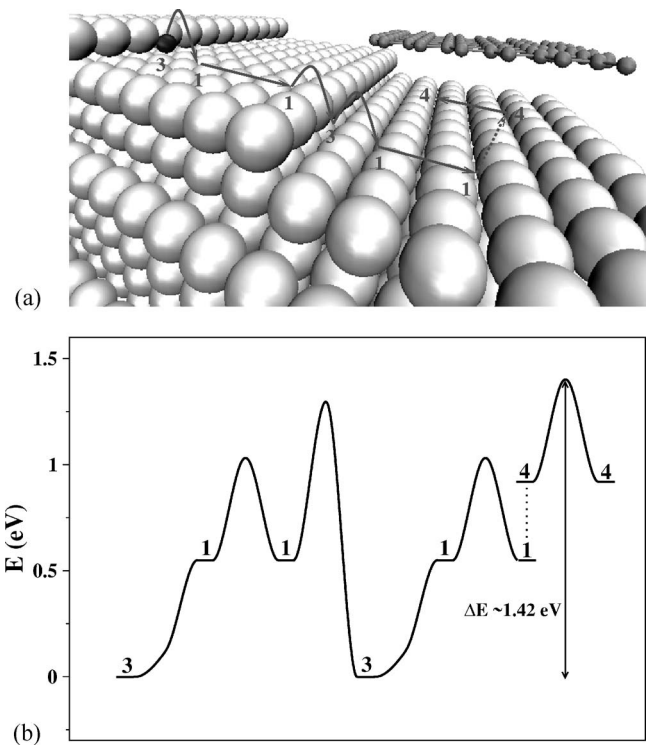


FIG. 5. (a) An illustration of the C diffusion steps on the Ni surface, including surface diffusion across a step. The light gray spheres constitute the graphite overlayer, whereas the dark gray sphere indicates the surface carbon adatom in its most favorable surface site. The white spheres indicate surface nickel atoms. The site numbering corresponds to the numbering of adsorption energies in Table I. The dotted line indicates the diffusion of carbon from the clean facet to the interface. (b) The calculated potential energy diagram for the C transport path in (a) with an indication of the overall transport energy barrier.

the fivefold hollow site below the step. A calculated barrier of 0.75 eV is obtained for this process. The upper panel of Fig. 5 shows the elementary steps in this transport pathway, and the lower panel of Fig. 5 shows the calculated energy diagram for the path. From the energy diagram we identify an overall transport energy barrier of 1.42 eV. This is similar to the barrier for the path including only facet diffusion reflecting that the destabilization due to the graphene overlayer has a larger impact than defects in the Ni surface.

2. Transport of carbon in the subsurface layers of nickel

The enhanced stability of C in the subsurface as compared to facet sites suggests that a step may also be passed by diffusion through the subsurface region, because the carbon atom will maintain a high metal coordination along such a path. However, an enhanced coordination of carbon in the subsurface layer will also lead to an increase in barrier for the diffusion event. Table II shows that the barrier for diffusion between the subsurface sites is clearly higher than the barrier for diffusion between sites at the (111) surface by 0.3 eV. In the transition state of the subsurface diffusion step, the surface Ni atoms relax outward by 0.63 Å as compared to their position on the fully relaxed, clean surface, to

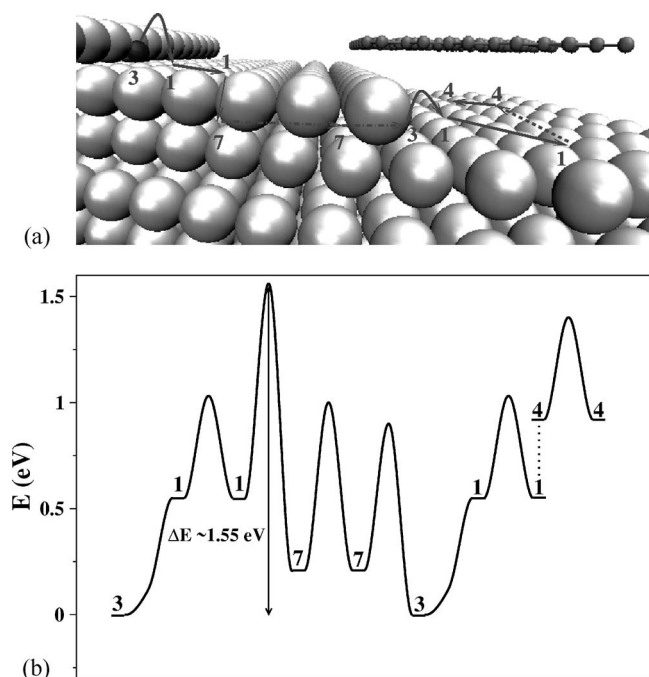


FIG. 6. (a) An illustration of the C diffusion steps on the Ni(111) surface, including subsurface diffusion. The light gray spheres constitute the graphite overlayer, whereas the dark gray sphere indicates the surface carbon adatom in its most favorable surface site. The white spheres indicate surface nickel atoms. The site numbering corresponds to the models in Table I. The dotted line indicates the diffusion of carbon from the clean facet to the interface. The dot-dashed lines illustrate the subsurface diffusion paths. (b) The calculated potential energy diagram for the C transport path in (a) with an indication of the overall transport energy barrier.

create room for the carbon atom. To map out the overall energetics, we consider the elementary steps in a subsurface transport path and the corresponding calculated energy diagram (see Fig. 6). The calculated energy barrier is found to be 1.55 eV. This is only 0.13 eV higher than for diffusion along the surface and is associated with the incorporation of the carbon atom into an octahedral subsurface site. The result indicates that subsurface migration could provide an alternative pathway for C to pass a step on the Ni surface.

Subsurface diffusion may also provide two different routes for carbon atoms to migrate from the step site to the nickel-graphene interface. In the first scenario, carbon diffuses away from the step to a facet site, incorporates into an octahedral site in the subsurface, diffuses along the subsurface, and finally jumps onto the graphene-nickel interface. The upper panel in Fig. 7 shows the elementary steps involved in the diffusion pathway and the lower panel in Fig. 7 shows the corresponding energy diagram. The total energy barrier is estimated to be 1.55 eV. The barrier increase as compared to the surface path in Fig. 4 is again seen to be associated with the step where carbon is incorporated into an octahedral subsurface site.

In the second scenario, carbon diffuses directly from the step site into an octahedral subsurface site, and then via the subsurface to the interface. The upper panel in Fig. 8 shows the elementary steps for the path, and the lower panel in Fig.

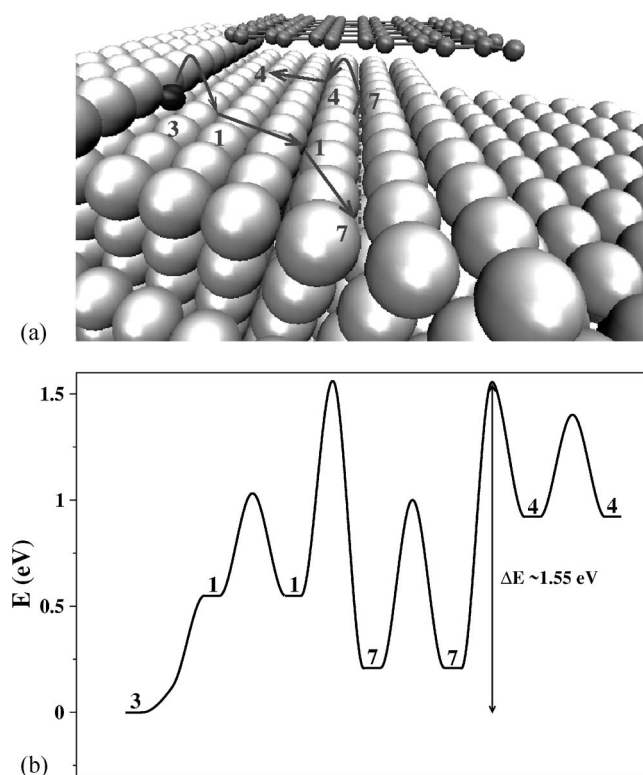


FIG. 7. (a) An illustration of the C diffusion steps on the Ni(111) surface, including subsurface diffusion directly onto the nickel-graphene interface. The light gray spheres constitute the graphite overlayer, whereas the dark gray sphere indicates the surface carbon adatom in its most favorable surface site. The white spheres indicate surface nickel atoms. The site numbering corresponds to the models in Table I. The dot-dashed line illustrates the subsurface diffusion path. (b) The calculated potential energy diagram for the C transport path in (a) with an indication of the overall transport energy barrier.

8 shows the corresponding potential energy diagram. From this, the overall transport energy barrier is found to be 1.55 eV.

3. Transport of carbon through the bulk of nickel

Finally, carbon diffusion through bulk nickel is considered. The calculations are done in the limit of a low carbon concentration using a unit cell containing 27 bulk nickel atoms per carbon atom. The energy barrier for diffusion between bulk octahedral sites is found to be 1.8 eV. This is considerably larger than for surface or subsurface diffusion steps, 0.5 eV and 0.8 eV, respectively. In the transition state, the nearest neighbor Ni atoms in the bulk are found to displace by 0.31 Å in the direction perpendicular to the (111) plane as compared to their position in the fully relaxed, clean Ni bulk. This is about half of the displacement found for the transition state associated with subsurface diffusion, indicating the enhanced stiffness of the bulk Ni lattice as compared to the surface Ni layer. Figure 9 shows the elementary steps in the diffusion path in the upper panel and the corresponding energetics can be viewed in the lower panel. The resulting overall activation energy for bulk diffusion of carbon is 2.33 eV.

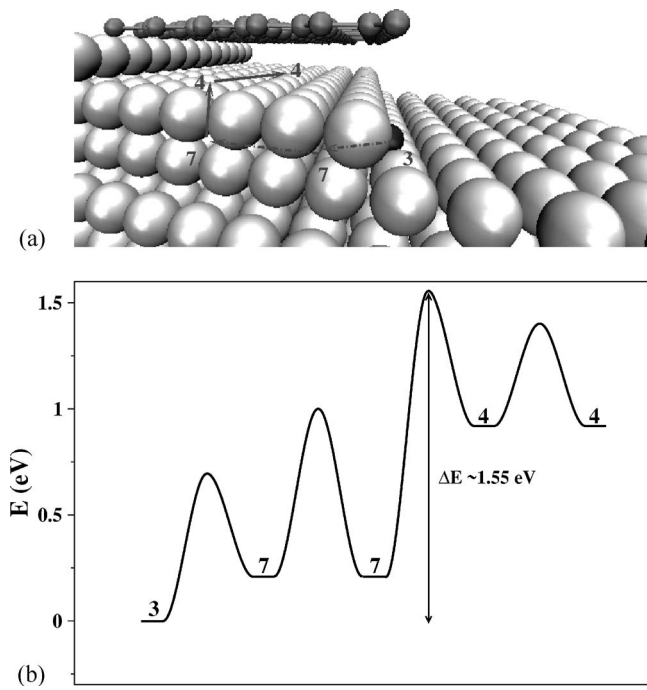


FIG. 8. (a) An illustration of the C diffusion steps on the Ni(111) surface, allowing for surface diffusion directly into the subsurface from the step and subsequently onto the nickel-graphene interface. The light gray spheres constitute the graphite overlayer, whereas the dark gray sphere indicates the surface carbon adatom in its most favorable surface site. The white spheres indicate surface nickel atoms. The site numbering corresponds to the models in Table I. The dot-dashed lines illustrate the subsurface diffusion paths. (b) The calculated potential energy diagram for the C transport path in (a) with an indication of the overall transport energy barrier.

4. Comparison of carbon transport mechanisms

The energy barriers for the different carbon diffusion paths from the free Ni surface to the graphene-nickel interface obtained from the model surfaces can now be compared. The overall activation energy barrier for diffusion of carbon atoms along the Ni surface is calculated to be 1.42 eV. The calculations show that the subsurface diffusion step of carbon is less favored (by approximately 0.30 eV) than the surface diffusion step and carbon experiences an increase in stability when adsorbed in subsurface octahedral sites of 0.34 eV relative to carbon adsorbed on the (111) facet. The overall barrier for the subsurface diffusion pathways are found to be 1.55 eV. The small difference between the calculated barriers along the surface or subsurface suggests that both mechanisms contribute and that C transport is confined to the surface region and proceeds as a multichannel process. Moreover, the calculations show that the bulk diffusion of carbon is associated with a significantly higher barrier, mainly due to an increased stiffness of the Ni lattice in the bulk. Hence, carbon diffusion along the surface, therefore, dominates carbon transport.

C. Graphene nucleation and growth

Sections IV A and IV B provided insight into the energetics of bonding and diffusion of C atoms at different Ni model

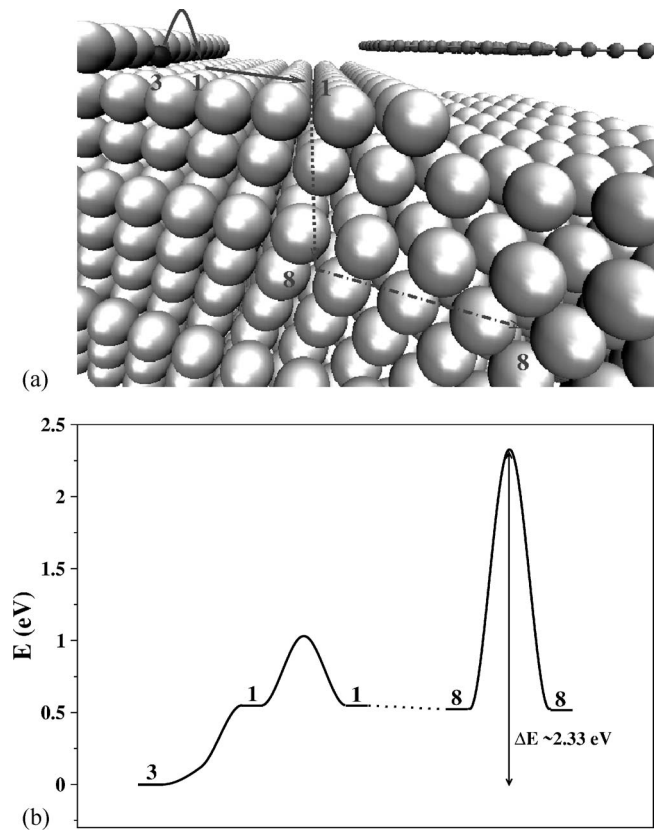


FIG. 9. (a) An illustration of the C diffusion steps on the Ni(111) surface, including diffusion into the bulk. The light gray spheres constitute the graphite overlayer whereas the dark gray sphere indicates the surface carbon adatom in its most favorable surface site. The white spheres indicate surface nickel atoms. The site numbering corresponds to the models in Table I. The dot-dashed line illustrates the bulk diffusion path. (b) The calculated potential energy diagram for the C transport path in (a) with an indication of the overall transport energy barrier.

surfaces. This section presents results from DFT calculations addressing the dynamics associated with the incorporation of C atoms into graphene structures adsorbed on the Ni surface. In accordance with Ref. 16, the step sites are regarded to act as the preferential nucleation sites for a graphene layer growing out over the lower-lying terrace. The growth continues as more C atoms are incorporated in the graphene layer either at perimeter sites located on the Ni(111) facet or perimeter sites at the step-edges of Ni. The free sp^2 orbitals at the perimeter of the graphene sheet are unstable and thus tend to bind to the Ni surface sites. Our calculations show that for carbon atoms at perimeter sites over the Ni facet, a bond is located at the threefold hollow sites, whereas carbon atoms at perimeter sites near the step-edge bond to a bridge site. The bond energy per carbon atom for the two different terminations differs by only 0.15 eV in favor of the facets.

1. Front growth at Ni facet sites

First, we consider the possibility of adding carbon atoms to the graphene perimeter located over the (111) facet on the nickel surface (see Fig. 10). In the initial state, the carbon

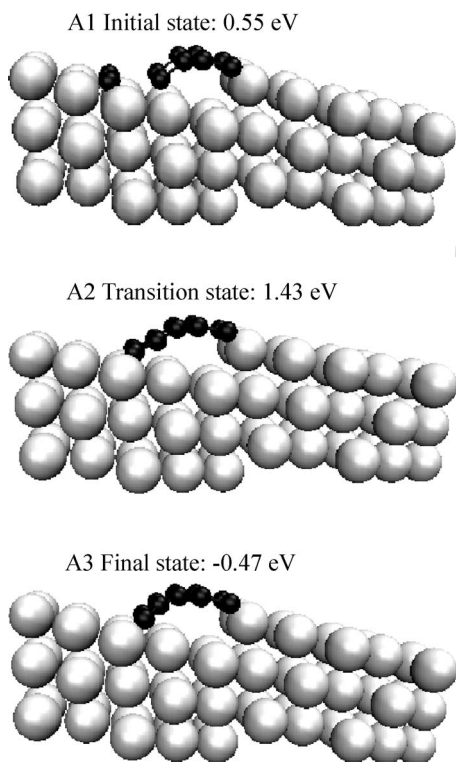


FIG. 10. Initial, transition, and final states in the front growth mechanism modeled in the DFT calculations. The energies are given per carbon atom relative to carbon adsorbed at the step (index 3 in Table I).

atoms are adsorbed in close proximity to the graphene perimeter. Specifically, the carbon atoms are adsorbed in adjacent threefold hollow sites on the Ni(111) terraces along the graphene perimeter. In the final state, the carbon atoms are incorporated in the graphene layer at perimeter sites. The reaction path between the initial and final states is identified using the NEB method on the Ni(322) model surface [Fig. 3(c)]. In the transition state, the carbon atoms are located just above a bridge site with the Ni surface atoms slightly lifted from the surface. The nickel surface relaxation tends to maintain a bond to the perimeter carbon atoms which move away from the surface to create room for the extra carbon atoms. The energy barrier for the incorporation of carbon is the energy difference between carbon situated near the perimeter in the initial state and the transition state and is found to be 0.88 eV per carbon atom. The overall activation energy for perimeter growth, with carbon initially adsorbed at the preferred step-edge adsorption site on the free Ni surface, is obtained as the sum of the barrier of 0.55 eV associated with the transportation of carbon from the step-edge site to the facet site in front of the graphene perimeter, and the barrier of 0.88 eV for incorporation of carbon. Figure 11 shows the energetics describing these elementary steps and identifies an overall energy barrier of 1.43 eV.

In the calculations, we have considered the addition of a chain of carbon atoms, located in adjacent hcp sites along the perimeter, to the graphene perimeter in a parallel process. Alternatively, the front growth could proceed by the addition

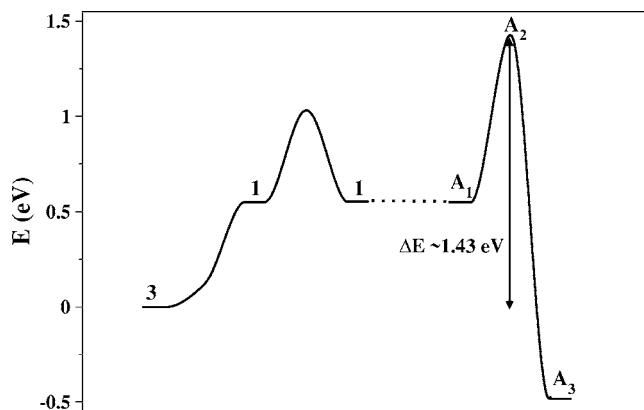


FIG. 11. Energy diagram for the elementary steps in the front growth mechanism of graphene layers on Ni surfaces. The indices are defined in Table I and Fig. 10. The arrow indicates the overall energy barrier for the front growth mechanism.

of single carbon atoms in a sequential process. Evidently, the graphene lattice in the vicinity of the incorporated carbon atom will be distorted and the addition of single carbon atoms is, therefore, expected to be associated with a slightly higher energy barrier.

2. Base growth by C incorporation

Incorporation of carbon into the graphene sheet may also occur at perimeter sites bonded to the nickel step edge. Such a base-growth scenario could proceed in a process in which (i) the graphene-nickel step-edge bonds are broken, (ii) the graphene layer is displaced away from the step to make room for the extra carbon atoms, and (iii) the graphene-step bonds are reestablished in a concerted motion by incorporation of extra carbon atoms into the graphene layer. The binding energy per carbon atom for a completely saturated step with a graphene overlayer is found to be 0.6 eV less stable than when adsorbed at the step edge on the graphene-free surface with $\theta_C^{\text{st}}=1$. Hence, in the following, we have considered carbon at the step edge as the initial state geometry. Figure 12 illustrates the initial, transition, and final states in the reaction.

The transition state is determined by employing the NEB method. We have used the 8×2 Ni(111) surface with five missing rows of surface Ni atoms to map out the transition. In the transition state, the step-edge nickel atoms are lifted from the surface to maintain a bond to the graphene layer, while a new bond between the carbon atoms to be incorporated is formed, thus ensuring a smooth transition. For the base growth, the energy barrier is 0.47 eV per carbon atom. The transition state energy is much lower than the C transport barrier; therefore, the full barrier for graphene growth on the Ni nanocluster is given as the energy required to bring carbon from the step edge on the graphene-free Ni surface to the nucleation center. Figure 13 shows the energetics associated with this which allows us to estimate the overall barrier for incorporation of carbon at the base to be 1.42 eV.

3. Base growth by atom exchange

The base of the graphene layer may provide a third mechanism for the addition of carbon atoms into the

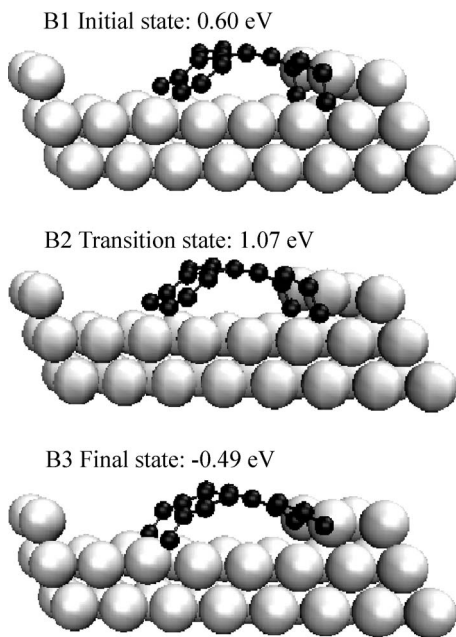


FIG. 12. Initial, transition, and final states in the base growth mechanism modeled in the DFT calculations. The energies are given per carbon atom relative to carbon adsorbed at the step edge (index 3 in Table I).

graphene layer. Contrary to the base growth by C incorporation, the nickel step-edge atoms are removed to make room for the carbon atoms which, in a concerted motion, are added to the graphene layer. Such an atom-exchange mechanism may proceed via the following route: Carbon diffuses to the step-edge site just below the graphene layer (Fig. 14) and then subsequently moves up into the graphene layer, while simultaneously expelling the nickel step-edge atom to the upper terrace where the next graphene layer in the graphite matrix stabilizes the nickel adatom.¹⁵ Such a calculation is computationally demanding, because it requires an optimization of more than 50 single atoms for each image along the reaction path, and therefore, we have been limited to an ap-

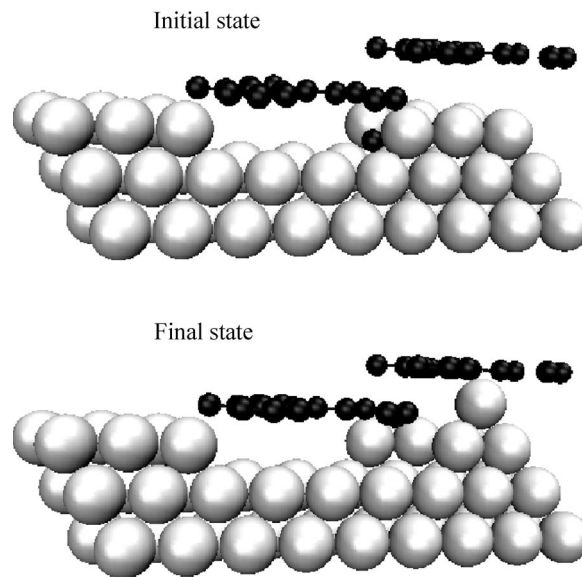


FIG. 14. Model of the initial and final states in an atom-exchange mechanism for base growth of graphene from a Ni step edge.

proximate scenario. In this scenario, the nickel step-edge atom is pushed onto the terrace below the terminated graphene layer. The 6×2 Ni(111) surface unit cell with three missing atomic rows, shown in Fig. 3(d), was used to identify the transition state and the energy barrier is found to be 0.54 eV (Fig. 15). Combined with the carbon transport barrier from a step site on the graphene-free surface to the graphene-nickel interface (Fig. 16), we estimate an overall barrier for the base growth of graphene by atom exchange to be 1.40 eV.

4. Comparison of the graphene growth mechanisms

The three different graphene growth mechanisms have similar activation energy barriers. This suggests that all three scenarios contribute to the graphene growth. In particular, the process involving base growth of graphene by C incorporation (Fig. 12) is seen to be rate-limited by carbon transport along the surface region. For the growth mechanisms where carbon is added to the front of graphene perimeter (Fig. 10) or to the base by atom exchange (Fig. 15), carbon transport along the surface and carbon incorporation contribute similarly to the barrier.

V. DISCUSSION

In the present DFT study, we have focused on the adsorption and diffusion of carbon atoms on nickel surfaces and the incorporation of carbon atoms into graphene layers. In combination with the previous study,¹⁵ we have established a consistent growth mechanism for multi-walled carbon nanofibers based on experimental observations and DFT calculations. Figure 2(b) illustrates the proposed mechanism. Nickel step-edge sites are identified as the preferential growth centers due to a stronger bonding of carbon atoms to such sites (Table I). The strong carbon bonding to the nickel

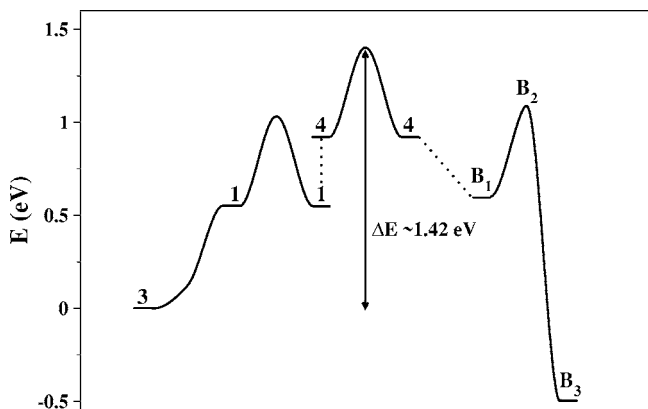


FIG. 13. Energy diagram for the elementary steps in the base growth of graphene layers on Ni surfaces by carbon incorporation at the Ni step edge. The indices are defined in Table I and Fig. 12. The arrow indicates the overall energy barrier for the base growth mechanism by C incorporation.

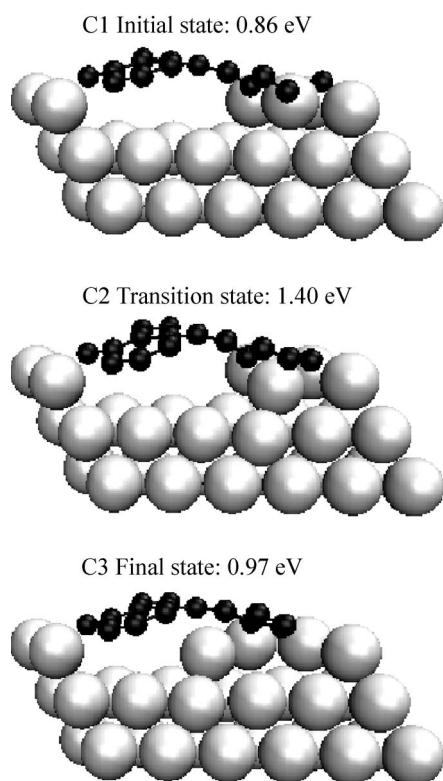


FIG. 15. Initial, transition, and final states in the atom-exchange growth mechanism modeled in the DFT calculations. The energies are given per carbon atom relative to carbon adsorbed at the step edge (index 3 in Table I).

step-edges explains why step-edges form spontaneously at the graphene-nickel interface, facilitating multilayered carbon nanofiber formation. Surface and interfacial transport mechanisms account for the removal of nickel from and the supply of carbon atoms to the graphene-nickel interface. Moreover, the calculations show that carbon transport may also occur along a subsurface path from the free nickel surface to the graphene-nickel interface, whereas bulk diffusion is unlikely to occur.

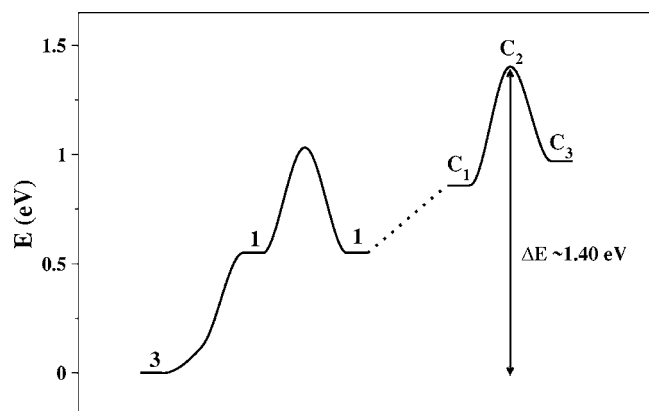


FIG. 16. Energy diagram for the elementary steps in the base growth of graphene layers on Ni surfaces by the atom-exchange mechanism. The indices are defined in Table I and Fig. 15. The arrow indicates the overall energy barrier for the base growth mechanism by atom exchange.

In the present growth model, the carbon transport along the Ni surface or subsurface to sites at the graphene-Ni interface is associated with an activation energy barrier of about 1.5 eV. The presence of carbon in the subsurface layer could have some effect on the adsorption and diffusion energy barriers of carbon at the surface. However, it is noticed that the barrier for diffusion of carbon in bulk Ni is 2.33 eV, which is considerably higher than for surface or subsurface transport, suggesting that carbon transport along the surface region should be dominating. Previous experimental studies find the activation energy barriers for bulk diffusion of carbon in the broad interval between 0.9 eV and 1.7 eV,^{32–34} which is well below the calculated value. As the diffusion energy barrier calculations are associated with an error of 0.25 eV,³⁵ it is more likely that the discrepancy is structural in origin. The DFT calculations use a single crystal model for the bulk carbon diffusion, as suggested by the *in situ* HR-TEM observations, whereas the previous experiments are carried out using polycrystalline nickel foils. Defects and grain boundaries in such foils are generally known to provide faster diffusion paths.^{36,37}

Moreover, the subsurface region was previously proposed to be of importance.^{38,39} It was suggested that a carbon concentration gradient is established in the subsurface region of the nanoclusters and acts as the driving force for carbon transport in a direction perpendicular to the Ni surface through the bulk nanocluster during steady-state growth. This is not in agreement with the present findings that diffusion inside the bulk cluster is highly unlikely. It should be noted that the previous models did not consider that C diffusion could occur along the surface in the subsurface layer.

So far we have provided a consistent picture, involving surface and subsurface diffusion, for the transport of carbon from the sites of deposition to the nucleation centers for graphene growth. Once carbon has reached these sites, the growth of graphene layers is initiated due to an energy gain when forming graphene islands on the surface. We have identified three mechanisms in which a continuous growth can be maintained, all of which may have implications for the specific graphitic structures. The front growth will only contribute as long as the graphene layer is oriented along the surfaces of the nanoclusters. In fact, growth via this mechanism might eventually encapsulate the particle completely. Growth via the two base mechanisms would also be expected to result in an encapsulation if the graphene layer growing along the Ni surface was unable to break its surface bonds. The energy required to break the graphene-step bonds is calculated to be 0.75 eV per carbon atom at the graphene perimeter. This is less than the 1.5 eV needed to incorporate the surface carbon atoms into the graphene overlayer. This indicates that detachment of graphene should happen spontaneously and this will lead to the formation of, e.g., nanofibers or nanotubes. The two base growth mechanisms may be important because they will continuously add carbon to the growing graphene layer. We speculate that both mechanisms could contribute to single-walled nanofiber and/or nanotube growth, whereas the atom-exchange mechanism is of importance to explain the experimentally observed mechanism for multi-walled nanofiber formation. The fact that all three growth mechanisms have similar activation energy barriers

suggests that they are associated with comparable growth rates and thus contribute to the same extent to the growth of graphitic structures. This may be one possible explanation for why growth of graphitic nanofiber structures often is observed to depend sensitively on the choice of catalyst and growth conditions.^{1,3} Moreover, the calculated activation energy barrier of about 1.5 eV is in good agreement with measured growth energy barriers in the range 1.3–1.5 eV.^{6,40}

Our results suggest that modifying the nickel step-sites could provide a way to control graphene formation. Additives, such as atomic sulfur, carbon, Ag and Au, all show a preference for adsorption at the steps on Ni(111),^{16,25,27,41} and it has been demonstrated that such additives will decrease the reactivity of methane reforming and at the same time block formation of graphitic structures at the steps.

VI. SUMMARY

In summary, DFT calculations are reported on carbon interaction with nickel surfaces providing a consistent interpretation of recent atomic-resolved *in situ* HRTEM observations of carbon nanofiber growth by methane decomposition over

nickel nanocrystals. The DFT results demonstrate that nickel step-edges are the preferred sites for carbon adsorption and act as growth centers for graphene layers. Transport of carbon from the step edge on the graphene-free Ni surface to the perimeter of the growing graphene layers is mediated by surface or subsurface diffusion, whereas diffusion of carbon through the bulk of the nickel nanocrystals are limited by a very high diffusion barrier. Our calculations identify three mechanisms for graphene growth: (i) front growth and (ii) base growth by C incorporation or (iii) atom-exchange at the Ni step edge. It is discussed how these mechanisms may explain encapsulation of the nanocrystals and the formation of single-walled and multi-walled graphitic nanofibres.

ACKNOWLEDGMENTS

F. A. P. and J. K. N. acknowledge support from the Danish National Research Foundation and the Danish Research Agency through Grant No. 26-04-0047. The DFT calculations have been performed with support from the Danish Center for Scientific Computing through Grant No. HDW-1103-06.

-
- ¹K. P. de Jong and J. W. Geus, *Adv. Catal.* **42**, 481 (2000).
²M. Terrones, *Int. Mater. Rev.* **49**, 6 (2004).
³K. Hata, D. N. Futaba, K. Mizuno, T. Numai, M. Yumura, and S. Iijima, *Science* **306**, 1362 (2004).
⁴P. M. Ajayan, *Chem. Rev. (Washington, D.C.)* **99**, 1787 (1999).
⁵J. R. Rostrup-Nielsen, J. Sehested, and J. K. Nørskov, *Adv. Catal.* **47**, 65 (2002).
⁶R. T. K. Baker, P. S. Harris, R. B. Thomas, and R. J. Waite, *J. Catal.* **26**, 51 (1972).
⁷J. R. Rostrup-Nielsen, *J. Catal.* **27**, 343 (1972).
⁸J. R. Rostrup-Nielsen and D. L. Trimm, *J. Catal.* **48**, 155 (1977).
⁹T. Baird, J. R. Fryer, and B. Grant, *Carbon* **12**, 591 (1974).
¹⁰H. E. Grenga and K. R. Lawless, *J. Appl. Phys.* **43**, 1508 (1972).
¹¹S. Hofmann, C. Ducati, J. Robertson, and B. Kleinsorge, *Appl. Phys. Lett.* **83**, 135 (2003).
¹²A. Oberlin, M. Endo, and T. Koyama, *J. Cryst. Growth* **32**, 335 (1976).
¹³R. Sharma and Z. Iqbal, *Appl. Phys. Lett.* **84**, 990 (2004).
¹⁴R. Sharma, P. Rez, M. Treacy, and S. Stuart, *J. Electron Microsc.* **54**, 231 (2005).
¹⁵S. Helveg, C. López-Cartes, J. Sehested, P. L. Hansen, B. S. Clausen, J. R. Rostrup-Nielsen, F. Abild-Pedersen, and J. K. Nørskov, *Nature (London)* **427**, 426 (2004).
¹⁶H. S. Bengaard, J. K. Nørskov, J. Sehested, B. S. Clausen, L. P. Nielsen, A. M. Molenbroek, and J. R. Rostrup-Nielsen, *J. Catal.* **209**, 365 (2002).
¹⁷L. Vitos, A. V. Ruban, H. L. Skriver, and J. Kollár, *Philos. Mag. B* **78**, 487 (1998).
¹⁸B. Hammer, L. B. Hansen, and J. K. Nørskov, *Phys. Rev. B* **59**, 7413 (1999).
¹⁹D. Vanderbilt, *Phys. Rev. B* **41**, R7892 (1990).
²⁰M. C. Payne, M. P. Teter, D. C. Allan, T. A. Arias, and J. D. Joannopoulos, *Rev. Mod. Phys.* **64**, 1045 (1992).
²¹J. L. F. Da Silva, C. Stampfl, and M. Scheffler, *Phys. Rev. Lett.* **90**, 066104 (2003).
²²R. Rosei, M. De Crescenzi, F. Sette, C. Quaresima, A. Savoia, and P. Perfetti, *Phys. Rev. B* **28**, 1161 (1983).
²³H. J. Monkhorst and J. D. Pack, *Phys. Rev. B* **13**, 5188 (1976).
²⁴G. Mills, H. Jónsson, and G. K. Schenter, *Surf. Sci.* **324**, 305 (1995).
²⁵R. T. Vang, K. Honkala, S. Dahl, E. K. Vestergaard, J. Schnadt, E. Lægsgaard, B. S. Clausen, and J. K. Nørskov, *Nat. Mater.* **4**, 160 (2005).
²⁶T. P. Beebe Jr., D. W. Goodman, B. D. Kay, and J. T. Yates Jr., *J. Chem. Phys.* **87**, 2305 (1987).
²⁷F. Abild-Pedersen, O. Lytken, J. Engbæk, G. Nielsen, I. Chorkendorff, and J. K. Nørskov, *Surf. Sci.* **590**, 127 (2005).
²⁸W. Humphrey, A. Dalke, and K. Schulten, *J. Mol. Graphics* **14**, 33 (1996).
²⁹U. Yxklintén, J. Hartford, and T. Holmquist, *Phys. Scr.* **55**, 499 (1997).
³⁰M. Todorova, W. X. Li, M. V. Ganduglia-Pirovano, C. Stampfl, K. Reuter, and M. Scheffler, *Phys. Rev. Lett.* **89**, 096103 (2002).
³¹We stress that, due to round off errors and differences in adsorption energies of carbon on the facet of the Ni(111) and Ni(211) model surfaces, the presented value differs slightly from the 1.6 eV reported in Ref. 15. The calculated barrier found is, nevertheless, still in good agreement with measured activation energies for carbon nanofiber growth.
³²J. J. Lander, H. E. Kern, and A. L. Beach, *J. Appl. Phys.* **23**, 1305 (1952).
³³T. A. Massaro and E. E. Petersen, *J. Appl. Phys.* **42**, 5534 (1971).
³⁴R. T. Yang and J. P. Chen, *J. Catal.* **115**, 52 (1989).
³⁵B. Hammer and J. K. Nørskov, *Adv. Catal.* **45**, 71 (2000).
³⁶D. C. Langreth, M. Dion, H. Rydberg, E. Schröder, P. Hyldgaard,

- and B. I. Lundqvist, *Int. J. Quantum Chem.* **101**, 599 (2005).
- ³⁷M. F. Ashby and D. R. H. Jones, *Engineering Materials: 1 An Introduction to their Properties and Applications* (Butterworth-Heinemann, Oxford, 2000).
- ³⁸I. Alstrup, *J. Catal.* **109**, 241 (1988).
- ³⁹J. W. Snoeck, G. F. Froment, and M. Fowless, *J. Catal.* **169**, 240 (1997).
- ⁴⁰D. L. Trimm, *Catal. Rev. - Sci. Eng.* **16**, 155 (1977).
- ⁴¹F. Besenbacher, I. Chorkendorff, B. S. Clausen, B. Hammer, A. M. Molenbroek, J. K. Nørskov, and I. Stensgaard, *Science* **279**, 1913 (1998).